Predicting tidal heights for extreme environments: From 25 hr observations to accurate predictions at Jang Bogo Antarctic Research Station, Ross Sea, Antarctica

Do-Seong Byun[1], Deirdre E. Hart[2]

[1]Ocean Research Division, Korea Hydrographic and Oceanographic Agency, Busan 49111, Republic of Korea
[2]School of Earth and Environment, University of Canterbury, Christchurch 8140, Aotearoa New Zealand

Correspondence to: Deirdre E. Hart (deirdre.hart@canterbury.ac.nz)

Abstract. Accurate tidal height data for the seas around Antarctica are much needed, given the crucial role of these tides in regional and global ocean, marine cryosphere, and climate processes. However obtaining long term sea level records for traditional tidal predictions is extremely difficult around ice affected coasts. This study evaluates the ability of a relatively new, tidal species based approach, the Complete Tidal Species Modulation with Tidal Constant Corrections (CTSM+TCC) method, to accurately predict tides for a temporary observation station in the Ross Sea, Antarctica, using records from a neighbouring reference station characterised by a similar tidal regime. Predictions for the 'mixed, mainly diurnal' regimes of Jang Bogo Antarctic Research Station (JBARS) were made and evaluated based on summertime (2017; and 2018 to 2019) short-term (25 hr) observations at this temporary station, along with tidal prediction data derived from year-long observations (2013) from the neighbouring 'diurnal' regime of Cape Roberts (ROBT). Results reveal the CTSM+TCC method can produce accurate (to within ~5 cm Root Mean Square Errors) tidal predictions for JBARS when using short-term (25 hr) tidal data from periods with higher than average tidal ranges (i.e. those at high lunar declinations). We demonstrate how to determine optimal short-term data collection periods based on the Moon's declination and/or the modulated amplitude ratio and phase lag difference between the diurnal and semidiurnal species predicted from CTSM at ROBT (i.e. the reference tidal station). The importance of using long period tides to improve tidal prediction accuracy is also considered and, finally, the unique tidal regimes of the Ross Sea examined in this paper are situated within a wider Antarctic tidal context using FES2014 model data.

1 Introduction

Conventionally, year-long sea level records are used to generate accurate tidal height predictions via harmonic methods (e.g. Codiga, 2011; Foreman, 1977; Pawlowicz et al., 2002). Obtaining long term records for such tidal analyses is extremely difficult for sea ice affected coasts like that surrounding Antarctica. As a compliment to in situ tidal records, recent work has significantly advanced our understanding of tide models for the shallow seas around Antarctica and Greenland via the assimilation of laser altimeter data and use of Differential Interferometric Synthetic Aperture Radar (DInSAR) imagery, amongst other methods (Padman et al., 2008; 2018; King et al., 2011; Wild et al., 2019). However, Byun and Hart (2015) developed a new approach to successfully predict tidal heights based on as little as 25 hr of sea level records when combined with neighbouring reference site records, using their Complete Tidal Species Modulation with Tidal Constant Corrections (CTSM+TCC) method, on the coasts of Korea and New Zealand. Demonstrating the usefulness of this method for generating accurate tidal predictions for new sites on sea ice affected coasts is the motivation for this study. We focus on the Ross Sea, Antarctica, as our case study area.

Long-term, quality sea level records in the Ross Sea are few and far between, and include observations from gauges operated by New Zealand at Cape Roberts (ROBT); by the United States in McMurdo Sound (see reference to data in Padman et al., 2003); and by Italy at Mario Zucchelli Station (Gandolfi, 1996), all in the eastern Ross Sea. Permanent sea level gauge installations in this extreme environment must accommodate or somehow avoid surface vents freezing over with sea ice, and damage to subsurface instruments from icebergs. There is also the challenge of securing and preventing damage to the cables that join the subsurface instruments to their onshore data loggers and power supplies, across the seasonally dynamic and harsh coastal and subaerial environments of Antarctic shorelines. At ROBT, these issues have been avoided by sheltering the sea level sensor towards the bottom of a 10 m long hole, drilled through a large, shoreline boulder, from its surface ~2 m above the sea and sea ice level, to ~6 m below sea level, below the base of the sea ice (Glen Rowe, Technical Leader Sea Level Data, New Zealand Hydrographic Authority, *pers. comm.* 13 Dec. 2019). In the absence of a suitable permanent gauge site, hydrographic surveys have been conducted at the Korean Jang Bogo Antarctic Research Station (JBARS). Such surveys are best conducted during the summertime predominantly sea ice free window around mid-January to mid-February. Even then, mobile ice (Fig. 1) and severe weather events frequently hinder surveys via instrument damage or loss, not to mention the logistical difficulties of instrument deployment and recovery (Rignot et al. 2000). Accurate tidal records from the Ross Sea and other areas around Antarctica are thus scarce compared to those available from other regions, although these data are much needed given the crucial role of tidal processes around this continent (Han et al., 2005; Jourdain et al., 2018; Padman et al., 2003; 2018).

Floating ice shelves occupy around 75% of Antarctica's perimeter (Padman et al., 2018). Tidal oscillations at the ice-ocean interface influence the location and extent of grounding zones (Padman et al., 2002; Rosier and Gudmundsson, 2018), and control heat transfer and ocean mixing in cavities beneath the marine cryosphere (Padman et al., 2018; Wild et al., 2019) and the calving and subsequent drift of icebergs (Rignot et al. 2000). Tides also affect variability in polynyas; patterns of seasonal sea ice; and thus the functioning of marine ecosystems. And tides affect the dynamics of landfast sea ice, which provides aircraft landing zones for Antarctic science operations (Han and Lee, 2018).

Accurate Antarctic region tidal input data are needed for models examining changes in global climate and ocean circulation, including for the generation of Antarctic bottom water (Han and Lee, 2018; Wild et al., 2019). Data on coastal tides are also essential for studies of ice mass balance and motion (Han and Lee, 2018; Padman et al., 2008; 2018; Rignot et al. 2000; Rosier and Gudmundsson, 2018; Wild et al., 2019). Ice thickness is typically measured via the subtraction of tidal height oscillations from highly accurate, but relatively low frequency, satellite based observations of ice surface elevation and/or from in situ Global Navigation Satellite System (GNSS) instrument observations (Padman et al., 2008). For floating ice, this procedure is relatively straightforward but where ice shelves and glacier tongues occur, the mechanics of grounding zones and ice flexure render the determination of ice thickness and motion challenging (Padman et al. 2018; Rosier and Gudmundsson, 2018), making the accuracy of tidal height inputs crucial for effective ice modelling (Wild et al. 2019).

In this study, we tested applicability of Byun and Hart's (2015) CTSM+TCC method in an extreme observation environment using 25 hr short-term records from JBARS, our temporary tidal observation station, and year-long data from ROBT, the neighbouring reference station. Sect. 2 of this paper details the JBARS and ROBT observation data sets used to generate harmonic tidal analysis results and CTSM+TCC tidal predictions. Sect. 3 explains how the CTSM+TCC method was applied and adapted in this case study (with Appendix 1 detailing the calculations), while Sect. 4 demonstrates the CTSM+TCC tidal prediction capability. Sect. 5 discusses the generation of fortnightly tide effects and double tidal peaks; and situates the Ross Sea tides examined in this paper within the wider context of Antarctic tidal regimes.

2 Antarctica's major tides: Observations and background

2.1 Study sites and data records

The Korea Hydrographic and Oceanographic Agency (KHOA) survey team went to JBARS in Northern Victoria Land's Terra Nova Bay, Ross Sea, Antarctica, in the austral summertime of 2017 (Fig. 2) for a preliminary fieldtrip to conduct hydrographic surveys and produce a nautical chart. This mission collected the first, 19 day sea level records for JBARS: 10 min interval observation data, recorded between 28 Jan. and 16 Feb. 2017 using a bottom-mounted pressure sensor (WTG-256S AAT, Korea). High-frequency sea level oscillations (<3 hr) were removed from the observation record using a fifth-order low-pass Butterworth filter. Note that the first and last days of this campaign comprised partial day records, so we excluded these end days from our tidal prediction experiments, since our method requires continuous 25 hr input data (for convenience, starting at midnight). That left 17 days and 1 hour of useable tidal observation data as the basis of the primary JBARS observation record.

For the purposes of a full-scale survey, three additional, discontinuous sea level observation records were measured by KHOA at JBARS between 29 Dec. 2018 and 11 Mar. 2019, all at 10 min intervals using the same instrument. Of these, the 20.54 day record produced between 29 Dec. 2018 and 18 Jan. 2019 comprised relatively high quality data with small residuals (i.e. observations minus predictions). We used this additional dataset (hereafter referred to as the JBARS 2019 observations) to verify CTSM+TCC method tidal predictions generated from input parameters derived from 'daily' (25 hr) slices of the 2017 sea level records. Due to the short duration of the KHOA survey team's forays into the Ross Sea, and in the absence of a permanent tide station at JBARS, it was not possible to collect the year-long sea level records that are commonly employed to obtain reliable tidal harmonic constants for tidal prediction.

Approximately 269 km south of JBARS, there is a permanent tidal observation station named after its location on Cape Roberts (ROBT), operated by Land Information New Zealand (LINZ) and recording at intervals since November 1990 (Fig. 2). Five minute interval sea level data have been collected at ROBT since November 2011 using Standard Piezometers (Model 4500, GEOKON). Part of the 2017 record from this site was unavailable online at the time of starting this research, so instead we chose as our reference records the 2013 ROBT sea level data, a quality year-long dataset with few missing points.

2.2 Tidal characteristic analyses and descriptions

Using the T_TIDE toolbox (Pawlowicz et al., 2002), we obtained the tidal harmonic constants of the 8 and 6 major tidal constituents for ROBT and JBARS, respectively (Table 1). Also the inference method was used to separate out neighbouring diurnal (K_1 and P_1) and semidiurnal (S_2 and K_2) tide constituents, with their amplitude ratios and phase lag differences obtained from harmonic analysis of the long-term ROBT reference station records. Analyses revealed that the two main diurnal (O_1 and K_1) and semidiurnal (M_2 and S_2) tides had similar amplitudes at the two stations, with the diurnal (semidiurnal) amplitudes being slightly larger (smaller) at ROBT than at JBARS, and the phase lags of all four tides having only slightly different values. The amplitude differences result in slightly different tidal form factors at the two sites (e.g., F in Table 1).

3 Using the CTSM+TCC tidal prediction methodology in the Ross Sea

Having analysed the tidal harmonic constants at the two stations, we then employed the CTSM+TCC method (Byun and Hart, 2015) to generate tidal height predictions for JBARS, our 'temporary' tidal observation station (subscript o), using ROBT as the 'reference' station (subscript r). This prediction approach (see Appendix 1 for the detailed calculations, and Byun and Hart (2015) for explanation of procedure development) is based on:

(i) using long-term (1 year, in our case) reference station records (LH_r) and CTSM calculations to make an initial anytime (τ) tidal prediction ($\eta_r(\tau)$), which involves summing tidal species' heights for the reference station (Fig.3);

(ii) comparing the tidal harmonic constants (amplitude ratios and phase lag differences) of representative tidal constituents (e.g., M_2 and K_1) for each tidal species between the temporary and reference stations, calculated using T_TIDE and concurrent short-term records (≥25 hr duration, starting at midnight) from the temporary (SH_o) and reference (SH_r) stations; and

(iii) using the step (ii) comparative data and the TCC calculations for each tidal species to adjust the $\eta_r(\tau)$ tidal species' heights in order to generate accurate, anytime tidal height predictions for the temporary tidal station ($\eta_o(\tau)$).

In this Ross Sea case study we used the 2017 JBARS tidal observation records (i.e. 17.04 days from 00:00 29 Jan. to 01:00 15 Feb.) as a source of SH_o, keeping the second JBARS 2019 observation record for evaluation purposes.

Importantly, this method assumes that the reference and temporary tidal stations are situated in neighbouring regimes with similar dominant tidal constituent and tidal species characteristics, and that the tidal properties between the two stations remain similar through time. As explained above, both JBARS and ROBT have tidal regimes that are primarily dominated by diurnal tides. LH_r must comprise high quality (e.g. few missing data) tidal height observations from anytime.

Byun and Hart (2015) recommended the use of short-term records gathered during periods of calm weather, to minimise errors due to atmospheric influences. They employed observational data for both SH_o and SH_r but as demonstrated in this paper the method can also be applied using tidal predictions as a source of SH_r. This adjustment in approach arose since for the 2017 JBARS observation time period, the concurrent 2017 ROBT records available online (LINZ, 2019) had multiple missing data. We solved this issue by producing a year-long synthetic 2017 record for ROBT using T_TIDE (Pawlowicz et al., 2002) and the 2013 (i.e. LH_r) observational record as input data. The 17.04 days of predicted tides that were concurrent with the 2017 JBARS observation record were then used as our SH_r source. While this CTSM+TCC method adjustment was procedurally small, it represents an important adaptation in the context of generating tidal predictions for stations situated in extreme environments, since concurrent temporary and reference station observations might be rare in such contexts.

When using CTSM+TCC, if the available temporary tidal station observation record covers multiple days, it is best practice to experiment by generating multiple $\eta_o(\tau)$, each using different concurrent pairs of SH_o and SH_r daily data slices in step (ii) above, to produce daily amplitude ratios and phase lag differences between the two stations for the diurnal K_1 and semidiurnal M_2 tidal constituents. Comparisons are then made between the different $\eta_o(\tau)$ data sets produced and the original temporary station observations, to determine the optimal 25 hr window to use: once selected, tidal height predictions can be generated for the temporary observation station for any time period. Thus, 17 individual 25 hr duration data slices were clipped from the 2017 JBARS observation records and from the concurrent ROBT predictions, forming 17 pairs of SH_o and SH_r 'daily' slices. Each paired data set was then used with LH_r to generate tidal height predictions for JBARS covering both the 2017 and 2019 KHOA observation campaign time periods. Comparisons were made between the JBARS observations and the 17 prediction data sets generated for each campaign to identify which 25 hr short-term data window produced optimal $\eta_o(\tau)$ results.

4 Results

4.1 Tidal prediction evaluation

CTSM+TCC was used to produce 17 different JBARS tidal prediction datasets for the period 29 Jan. to 14 Feb. 2017, based on harmonic analysis results of the 'daily' (25 hr) K_1 and M_2 amplitudes and phase lags at our two tidal observation stations (Fig. 4). In order to evaluate these results, each predicted tidal height data set was compared with the concurrent JBARS field observations via Root Mean Square Error (RMSE) and coefficient of determination (R^2) statistics. As illustrated in Fig. 5, the RMSE and R^2 results varied in relation to the JBARS tidal range (range being twice amplitude), with greater accuracy evident in predictions made using data derived from periods with above average tidal ranges.

In the JBARS area of the Ross Sea during our 2017 observation period, above average tidal ranges corresponded to the period when the moon was near its greatest northern declination. RMSEs between observations and predictions ranged from 4.26 cm to 20.56 cm, while R^2 varied from 0 to 0.94, across the 17 'daily' experiments. Eleven of the experiments produced accurate results (i.e. excluding those derived from 31 Jan.; and 1 to 4 and 14 Feb. data slices). Daily datasets from periods with relatively high tidal ranges (>83.5 cm) produced predictions with RMSEs <5 cm and R^2 values >0.92. The maximum spring tidal range occurred on 9 Feb.: the data slices from this date produced predictions with a low (but not the lowest) RMSE (4.81 cm). The predictions with the lowest RMSE (4.259 cm) and highest R^2 value (0.941) were produced using data slices from one day earlier, 8 Feb. 2017. In contrast to the majority of successful experiments, the experiment based on data derived from the 2 Feb. 2017 data slices produced predictions with very high RMSE (20.56 cm) and very low R^2 (0.00) values. The 2 Feb. 2017 tides were characterised by the smallest tidal range (11.95 cm) of the JBARS record, during a period of low lunar declination. As with the 2017 predictions, RMSEs between the 2019 predictions and observations were lower when generated using data slices from 2017 periods at high lunar declination (Fig.6). For example, 2019 predictions made using input data derived from the 8 Feb. 2017 data slices produced the lowest RMSE (5.3 cm) and highest R^2 (0.913) values of the 2019 experiments (Fig. 7).

These results show that the CTSM+TCC method can be used successfully to predict tidal heights for JBARS, when using observation records gathered from periods at high lunar declination (sometimes called tropic tides), with relatively calm weather, together with observation or prediction records from the neighbouring reference station ROBT.

4.2 Determining the ideal short-term sea level observation period when using CTSM+TCC

The previous section verified that the CTSM+TCC method can be used to generate accurate tidal predictions based on 25 hr sea level records, from periods with above average tidal ranges, for a temporary station in a mixed, mainly diurnal regime and a reference station in a diurnal regime. The question arises as to how to determine optimal observation days in such settings to produce the most accurate tidal predictions.

For semidiurnal or mixed, mainly semidiurnal tidal regimes, we can estimate preferred temporary station observation days, those with the largest tidal ranges, based on the moon's phase, without reference to tide tables. That is, spring tides commonly occur just a day or two after the full and new moon, which reoccurs at a period of 14.76 days. The time lag between the full or new moon and the spring tide is called the age of the tide (*AT*).

Similarly, in a diurnal tide regime or a mixed, mainly diurnal tide regime (Fig. 5), preferred temporary station observation days can be estimated based on the lunar declination, which varies at a period of 13.66 days. That is, maximum tidal range days can be estimated for JBARS based on the day of the Moon's greatest northern (GN) and southern (GS) declinations. The time between the Moon's semi-monthly GN and GS declinations and their effects on tidal range, called the age of diurnal inequality (*ADI*), is commonly 1 to 2 days. As shown in Fig. 8, the GN and GS lunar declinations during our temporary station summertime observation periods occurred on 8 Feb. 2017 (GN) and on 6 Jan. 2019 (GS) respectively, with the maximum diurnal tides at JBARS expected around 1 day after each lunar declination peak.

Thus, when planning to use the CTSM+TCC tidal prediction method for places characterised by diurnal or mixed, predominantly diurnal tidal regimes, we can use knowledge of the moon's declination to select potential sea level observation days.

4.3 Comparison of ROBT and JBARS tidal species characteristics

The CTSM+TCC tidal prediction method is based on the assumption that the tidal harmonic characteristics of each tidal species are very similar between the temporary and reference stations. This is because the reference station tidal species' CTSMs form the basis of the tidal predictions for the temporary observation station. To test the validity of this assumption, we examined the phase lag (*G*) differences of the two major diurnal and semidiurnal tidal constituents using *ADI* and *AT*, calculated as:

$$ADI\ (day) = \left(\frac{G_{K_1} - G_{O_1}}{\omega_{K_1} - \omega_{O_1}}\right)/24 \text{ , and} \quad (1)$$

$$AT\ (day) = \left(\frac{G_{S_2} - G_{M_2}}{\omega_{S_2} - \omega_{M_2}}\right)/24 \text{ ,} \quad (2)$$

where ω_{K_1} (= 15.0410686° hr^{-1}), ω_{O_1} (= 13.9430356° hr^{-1}), ω_{S_2} (= 30.0000000° hr^{-1}), and ω_{M_2} (= 28.9841042° hr^{-1}) are the angular speeds of the K_1, O_1, S_2 and M_2 tides, respectively. Results revealed that the *ADI* are very similar, and there is <1 day *AT* difference, between ROBT and JBARS respectively (Table 1), indicating that the tidal characteristics of the representative tidal constituents for each species between the two stations are very similar, in particular the dominant diurnal species. This similarity explains why we found the CTSM+TCC method successful in generating our Ross Sea tidal predictions.

5 Discussion

5.1 Explaining fortnightly tide effects and double tide peaks in the Ross Sea tidal predictions

We have demonstrated that the CTSM+TCC approach can produce reasonably accurate tidal predictions (RMSE <5 cm, R^2 >0.92) for a new site in the Ross Sea, Antarctica, based on 25 hr temporary station observation records from periods with above average tidal ranges, plus neighbouring reference station records. Our results compare favourably with those of Han et al. (2013), who reviewed the tidal height prediction accuracy of 4 models for Terra Nova Bay, Ross Sea: these models generated similar quality results to our CTSM+TCC results, with R^2 values between 0.876 and 0.907, and RMSEs ranging from 3.6 to 4.1 cm. However, as shown in Fig. 7, our results contain a changing fortnightly timescale bias in estimates. This error pattern likely resulted from our application of CTSM+TCC considering only 2 major tidal species (diurnal and semidiurnal) whilst ignoring several long period and small amplitude short period tides.

Table 2 summarises the characteristics of 6 long-period tides (S_a, S_{sa}, MS_m, M_m, M_f, MS_f) at the ROBT station, derived from tidal harmonic analysis of year-long (2013) in situ observation records. To investigate the main cause of the apparent fortnightly prediction biases in our JBARS results, in particular that in the 2019 predictions (Fig. 7b), we examined the effects of two fortnightly tidal constituents (M_f, and MS_f) at ROBT. Three 2019 tidal prediction experiments were conducted:

- *Srun* excluded all long-period tides (see list of exclusions in Table 2);
- *Run1* was based on *Srun* but also incorporated the M_f; and
- *Run2* was based on *Srun* but also incorporated the M_f and MS_f.

Comparisons between *Run1 and Srun* predictions show that exclusion of the M_f tide (2.7 cm amplitude) can produce prediction biases during periods of lunar declination change (Fig. 9a), with comparisons between *Run2 and Run1* results showing that the additional exclusion of the MS_f tide (1.2 cm amplitude) intensifies the biases (Fig. 9b).

Rosier and Gudmundsson (2018) found that ice flows are modulated at various tidal frequencies, including that of the MS_f tide. However, because these tides' amplitudes have small signal-to-noise ratios (<1) with large standard errors (Table 2), caution should be exercised when elucidating fortnightly tide effects using these constituents. Nevertheless, studies indicate that incorporating major and minor tidal constituents, including long period tides, into tidal predictions may be advantageous for their use in ice flow and ice-ocean front modelling specifically (e.g. Rignot et al., 2000; Rosier and Gudmundsson, 2018). Consideration of additional, long period tides in predictions is one recommendation we have for future work on improving tidal predictions for Ross Sea coasts.

Another characteristic of our results needing explanation is the double tidal peaks evident in both the tidal observations and predictions at JBARS. These peaks occur, for example, in Fig. 7b between Jan. 11th and 17th, 2019. To explore why these double peaks occur, we generated JBARS tidal height predictions using Eq. (A1) and the 2019 tidal constants listed in Table 1 for the two major diurnal and semidiurnal tides. Fig. 10a shows separately the resulting diurnal (with their period of 13.66 days) and semidiurnal (with their period of 14.77 days) species' tide predictions. The combination of these out-of-phase tidal species generates double peaks (or double troughs) around low tide (Fig. 10b) for periods when the diurnal tide amplitudes are low, and the amplitude ratio of the semidiurnal to diurnal tide species is >0.5 (Fig. 10c). Double peaks also occur around high tide during periods of low lunar declination (Fig. 8b), when the semidiurnal to diurnal species amplitude ratio is >1, and the phase lag difference between the diurnal and semidiurnal species is between -78° and 46° (Fig. 10). Since the semidiurnal tides are slightly stronger, and the diurnal tides are slightly weaker, at JBARS compared to at ROBT (Table 1), these double tide peaks occur more commonly at JBARS (e.g., compare Fig. 5b and Fig. 7).

5.2 Understanding the contrasting tidal environments around Antarctica

Figure 11 illustrates the form factors of tidal regimes in the seas surrounding Antarctica, according to FES2014 model data. There are large areas characterised by diurnal (F>3); mixed, mainly diurnal (1.5<F<3); and mixed, mainly semidiurnal (0.25<F<1.5) forms. Only in a small area half-way along the Weddell Sea coast of the Antarctic Peninsula (at 72°S) do tides exhibit a semidiurnal form (F<0.25). Strong diurnal tides predominate in the Ross Sea area of West Antarctica, around to the Amundsen Sea. In addition, a small area near Prydz Bay (Fig. 2) in East Antarctica exhibits diurnal and mixed mainly diurnal tides. The rest of the seas surrounding Antarctica, including the Weddell Sea, are predominantly characterised by mixed, mainly semidiurnal tides.

Since diurnal tides have larger nodal amplitude factor and nodal angle variations than semidiurnal tides (Pugh and Woodworth, 2014), areas like the Ross Sea will have larger variations in tidal height across the 18.61 year lunar nodal cycle compared to areas like the Weddell Sea. As the nodal angle variations of the diurnal and semidiurnal tides are out of phase, this leads to differing tidal responses around Antarctica over 18.61 years, particularly between the Ross and Weddell Seas (see details for ROBT in Byun and Hart, 2019). Given that CTSM+TCC is based on modulated tidal amplitude and phase lag corrections for each diurnal and semidiurnal species, it is applicable in studying a continent with such a diversity of tidal regime types. Accurate (cm scale) quantification of the contrasting tidal behaviours and environments around Antarctica's margins are not only of use for polar station maritime operations, they are essential for estimating ice flows to the sea. This paper has shown how the CTSM+TCC approach may be used to complement existing efforts to quantify variations in tidal processes around Antarctica, in particular for places with sparse in situ tidal monitoring, such as the Ross Sea.

6 Conclusions

This paper has demonstrated the usefulness of the CTSM+TCC method for tidal prediction in extreme environments, where long-term tidal station installations are difficult, using the Ross Sea in Antarctica for our case study. Here CTSM+TCC methods can be employed for accurate tidal height predictions for a temporary tidal observation station using short-term (≥25 hr) sea level records from this site, plus long-term (1 year) tidal records from a neighbouring reference tidal station. Essentially the temporary and reference station sites must share similarities in their main tidal constituent and tidal species characteristics for CTSM+TCC to produce acceptable results.

Using this approach, an initial tidal prediction time series is generated for the temporary station using CTSM and the reference station long-term records. The temporary station predicted time series can then be adjusted via TCC of each tidal species, based on harmonic comparisons between the short-term temporary station observation record and its corresponding modelled predictions, leading to improved accuracy in the tidal predictions. The modulated amplitude ratio and phase lag difference between diurnal and semidiurnal species predicted from CTSM at the reference station can be used as an indicator for selecting optimal short term observation dates at a temporary tidal station.

This paper has further demonstrated that the CTSM+TCC approach can be employed successfully in the absence of concurrent short-term (25 hr) records from the reference station, since a tidal harmonic prediction program can be used to produce a synthetic short-term record for the reference station, based on a quality long-term (1 year) record from that site.

The proper consideration of long-period tides in the CTSM+TCC approach remains a challenge, as outlined in this study, with the solutions to this issue likely to improve tidal predictions further. However, this study demonstrates that the CTSM+TCC method can already produce tidal predictions of sufficient accuracy to aid local polar station maritime operations, as well as starting to help resolve gaps in the spatial coverage of tidal height predictions for scientists studying important issues, such as the rate and role of ice loss along polar coastlines.

Code Availability

The T_TIDE based CTSM code is available from https://au.mathworks.com/matlabcentral/fileexchange/73764-ctsm_t_tide.

Data Availability

The sea level data used in this paper are available from LINZ (2019) for selected ROBT records, with the remaining ROBT records available by email application (customersupport@linz.govt.nz); and the JBARS records used are available on request from KHOA (infokhoa@korea.kr). Details of the FES2014 tide model are found in Carrère et al. (2016) and via https://www.aviso.altimetry.fr/en/data/products/auxiliary-products/global-tide-fes.html.

Appendix 1

This appendix describes the calculations involved in using the CTSM+TCC approach as employed in this Ross Sea, Antarctica, case study. For a fuller description of the development of this approach and its application in semidiurnal and mixed, mainly semidiurnal tidal regime settings, see Byun and Hart (2015).

As explained in the main body of this paper, we used 25 hr slices of the 2017 short-term observations from JBARS (SH_o), our temporary tidal observation station (subscript *o*), and 2013 year-long observations (LH_r) and 2017 short-term tidal predictions (SH_r, concurrent with SH_o) from ROBT, our reference tidal station (subscript *r*), as the basis of JBARS tidal prediction calculations. We then employed the full 17.04 day 2017 JBARS tidal observation data set, and an additional 21.54 day 2019 JBARS tidal observation dataset, to evaluate the success of the CTSM+TCC tidal prediction calculations for this site.

The CTSM+TCC, expressed as the summation of each tidal species cosine function, includes three key steps:

(i) calculating each tidal species' modulation at the reference tidal station;

(ii) comparing the tidal harmonic constants between the temporary observation and reference stations (e.g., the tidal amplitude ratios and phase lag differences of each representative tidal constituent for each tidal species calculated from concurrent observation records between two stations); and

(iii) adjusting the tidal species modulations calculated in the first step using the correction factors calculated in the second step to produce predictions for the temporary tidal station.

As a first step, tidal height predictions for the temporary station ($\eta_o(\tau)$) were initially derived from reference station predictions ($\eta_r(\tau)$) on the assumption that the tidal properties between the two stations remain similar through time. Using the modulated amplitude ($A_r^{(s)}$) and the modulated phase lag ($\varphi_r^{(s)}$) for each tidal species, this step is expressed as:

$$\eta_r(\tau) = \sum_{s=1}^{k} A_r^{(s)}(\tau) \cos\left(\omega_R^{(s)} t - \varphi_r^{(s)}(\tau)\right) \quad \text{(A1)}$$

with

$$A_r^{(s)}(\tau) = \sqrt{\sum_{i=1}^{m}\left[f(\tau)_i^{(s)} a_i^{(s)}\right]^2 + 2\sum_{i=1}^{m-2}\sum_{j=i+1}^{m}\left[f(\tau)_i^{(s)} a_i^{(s)}\right]\left[f(\tau)_j^{(s)} a_j^{(s)}\right]\cos\left\{\left(\omega_i^{(s)} - \omega_j^{(s)}\right)t + \left[V(t_0)_i^{(s)} + u(\tau)_i^{(s)} - G_i^{(s)}\right] - \left[V(t_0)_j^{(s)} + u(\tau)_j^{(s)} - G_j^{(s)}\right]\right\}}$$

(A2)

and

$$\varphi_r^{(s)}(\tau) = tan^{-1}\left(\frac{\sum_{i=1}^{m} a_i^{(s)} \sin[(\omega_i^{(s)} - \omega_R^{(s)})t + V(t_0)_i^{(s)} + u(\tau)_i^{(s)} - G_i^{(s)}]}{\sum_{i=1}^{m} a_i^{(s)} \cos[(\omega_i^{(s)} - \omega_R^{(s)})t + V(t_0)_i^{(s)} + u(\tau)_i^{(s)} - G_i^{(s)}]}\right) \quad \text{(A3)}$$

where superscript *s* denotes the type of tidal species (e.g., 1 for diurnal species and 2 for semidiurnal species); *m* is the number of tidal constituents; t_0 is the reference time; *t* is the time elapsed since t_0; and $\tau = t_0 + t$; $\omega_i^{(s)}$ are the angular frequencies of each tidal constituent (subscripts *i* and *j*); $\omega_R^{(s)}$ are the angular frequencies of each tidal constituent representing a tidal species (subscript *R*); with the dominant tidal constituent of each tidal species used as the representative for that species (e.g., K_1 and M_2 are used as representative of the diurnal and semidiurnal species, respectively). For each tidal constituent, $a_i^{(s)}$ and $G_i^{(s)}$ are the tidal harmonic amplitudes and phase lags (referenced to Greenwich); $f(\tau)_i^{(s)}$ is the nodal amplitude factor of each tidal constituent; $u(\tau)_i^{(s)}$ is the nodal angle; and $V(t_0)_i^{(s)}$ is the astronomical argument. T_TIDE was used for tidal harmonic analysis as well as for calculation of the nodal amplitude factors; nodal angles; and astronomical arguments; for the representative tidal constituents.

As the second step, under the 'credo of smoothness' assumption that the admittance or 'ratio of output to input' does not change significantly between constituents of the same species (Munk and Cartwright, 1966; Pugh and Woodworth, 2014), the amplitude ratio and phase lag difference of each representative tidal constituent for each tidal species between the temporary and reference stations were calculated from the results of tidal harmonic analyses of concurrent 25 hr data slices (starting at

00.00) from the temporary observation and reference tidal stations (i.e. from SH_o and SH_r). The process of selecting the optimal 25 hr window for the concurrent data slices from amongst the 17.04 days of available records is explained in Sect. 3. Once this 2017 window was selected, the third step involved adjusting the tidal predictions at the reference station calculated from Eq. (A1), to represent those for the temporary station ($\eta_o(\tau)$), by substituting the daily (i.e. SH_o and SH_r) amplitude ratios $\left(\frac{a_o^{(s)}}{a_r^{(s)}}\right)$ and phase lag differences $\left(G_o^{(s)} - G_r^{(s)}\right)$ for the tidal constituents (K_1 and M_2) representing the diurnal and semidiurnal tidal species between the temporary and reference stations into Eq. (A1) as follows (Byun and Hart, 2015):

$$\eta_o(\tau) = \sum_{s=1}^{k} A_o^{(s)}(\tau)\cos\left(\omega_R^{(s)} t - \varphi_o^{(s)}(\tau)\right) \quad \text{(A4)}$$

with $A_o^{(s)}(\tau) = A_r^{(s)}(\tau)\left(\frac{a_o^{(s)}}{a_r^{(s)}}\right)$, and (A5)

$$\varphi_o^{(s)}(\tau) = \varphi_r^{(s)}(\tau) + G_o^{(s)} - G_r^{(s)} \quad \text{(A6)}$$

Substituting Eqs. (A5) and (A6) into Eq. (A4), $\eta_o(\tau)$ can be expressed as:

$$\eta_o(\tau) = \sum_{s=1}^{k} A_r^{(s)}(\tau)\left(\frac{a_o^{(s)}}{a_r^{(s)}}\right)\cos\left[\omega_R^{(s)} t - \left(\varphi_r^{(s)}(\tau) + G_o^{(s)} - G_r^{(s)}\right)\right] \quad \text{(A7)}$$

The T_TIDE based CTSM code is available from https://au.mathworks.com/matlabcentral/fileexchange/73764-ctsm_t_tide.

Author contribution

D-SB conceived of the tidal prediction idea behind this paper, and wrote the results sections. Both authors worked on initial and final versions of the full manuscript.

Competing interests

The authors declare that the research was conducted in the absence of any commercial or financial relationships that could be construed as a potential conflict of interest.

Special issue statement (will be included by Copernicus)

Acknowledgements

We are grateful to Land Information New Zealand (LINZ) and the Korea Hydrographic and Oceanographic Agency (KHOA) for supplying the tidal data used in this research. A special thank you to Glen Rowe from LINZ for sharing his extensive knowledge of the Cape Roberts sea level gauge site and its records, and to a KHOA colleague for providing the Fig. 1 photograph. Further, we gratefully thank Ms. Hyowon Kim at KHOA for her kind assistance with drafting figures. We are also grateful to Philip Woodworth, Glen Rowe and an anonymous reviewer for comments that greatly helped us improve our manuscript.

References

Byun, D.-S. and Hart, D. E.: On robust multi-year tidal prediction using T_TIDE, Ocean Sci. J., 54, 685-691, doi.org/10.1007/s12601-019-0028-4, 2019.

Byun, D.-S. and Hart, D. E.: Predicting tidal heights for new locations using 25h of in situ sea level observations plus reference site records: A complete tidal species modulation with tidal constant corrections, J. Atmos. Ocean. Tech., 32, 350-371, doi.org/10.1175/JTECH-D-14-00030.1, 2015.

Carrère L., Lyard, F., Cancet, M., Guillot, A. and Picot, N.: FES 2014, a new tidal model - validation results and perspectives for improvements, Presentation to ESA Living Planet Conference, Prague, 2016.

Codiga, D. L.: Unified Tidal Analysis and Prediction Using the UTide Matlab Functions, Technical report 2011-01, Graduate School of Oceanography, University of Rhode Island, 2011.

Foreman, M. G. G.: Manual for Tidal Heights Analysis and Prediction, Pacific Marine Science Report, 77-10, 1977.

Gandolfi, S.: Terra Nova Bay Permanent Tide Gauge Observatory Site, https://www.geoscience.scar.org/geodesy/perm_ob/tide/terranova.htm, last access 4 Feb. 2020, 1996.

Han, H. and Lee, H.: Glacial and tidal strain of landfast sea ice in Terra Nova Bay, East Antarctica, observed by interferometric SAR techniques, Remote Sens. Environ., 209, 41–51, doi.org/10.1016/j.rse.2018.02.033, 2018.

Han, H., Lee, J., and Lee, H.: Accuracy assessment of tide models in Terra Nova Bay, East Antarctica, for glaciological studies of DDInSAR technique, Korean Journal of Remote Sensing, 29, 375–387, 2013.

Han, S. C., Shum, C. K., and Matsumoto, K.: GRACE observations of M2 and S2 ocean tides underneath the Filchner-Ronne and Larsen ice shelves, Antarctica, Geophys. Res. Lett., 32, L20311, doi.org/10.1029/2005GL024296, 2005.

Jourdain, N. C., Molines, J.-M., Le Sommer, J., Mathiot, P., Chanut, J., de Lavergne, C., and Madec, G.: Simulating or prescribing the influence of tides on the Amundsen Sea ice shelves, Ocean Model., 133, 44–55, doi.org/10.1016/j.ocemod.2018.11.001, 2018.

King, M. A., Padman, L., Nicholls, K., Clarke, P. J., Gudmundsson, G. A., Kulessa, B., and Shepherd, A.: Ocean tides in the Weddell Sea: New observations on the Filchner-Ronne and Larsen C ice shelves and model validation, J. Geophys. Res., 116, C06006, doi.org/10.1029/2011JC006949, 2011.

LINZ, Land Information New Zealand: Sea level data downloads, http://www.linz.govt.nz/sea/tides/sea-level-data/sea-level-data-downloads, last access 2019.

Munk, W. H. and Cartwright, D. E.: Tidal spectroscopy and prediction, Math. Phys. Sci., 259, 533-581, doi.org/10.1098/rsta.1966.0024, 1966.

Padman, L., Erofeeva, S., and Fricker, H.: Improving Antarctic tide models by assimilation of ICESat laser altimetry over ice shelves, Geophys. Res. Lett., 35, l22504, doi.org/10.1029/2008GL035592, 2008.

Padman, L., Erofeeva, S., and Joughin, I.: Tides of the Ross Sea and Ross Ice Shelf cavity, Antarct. Sci., 15, 31–40, doi.org/10.1017/S0954102003001032, 2003.

Padman, L., Fricker, H., Coleman, R., Howard, S., and Erofeeva, L.: A new tide model for the Antarctic ice shelves and seas, Ann. Glaciol., 34, 247–254, doi.org/10.3189/172756402781817752, 2002.

Padman, L., Siegfried, M., and Fricker, H.: Ocean Tide Influences on the Antarctic and Greenland Ice Sheets, Rev. Geophys., 56, 142–184, doi.org/10.1002/2016RG000546, 2018.

Pawlowicz, R., Beardsley, B., and Lentz, S.: Classical tidal harmonic analysis including error estimates in MATLAB using T_TIDE, Comput. Geosci., 28(8), 929-937, doi.org/10.1016/S0098-3004(02)00013-4, 2002.

Pugh, D. T.: Tides, Surges and Mean Sea-Level: A Handbook for Engineers and Scientists, Wiley, Chichester, United Kingdom, 1987.

Pugh, D. T. and Woodworth, P. L.: Sea-level science: Understanding tides, surges, tsunamis and mean sea-level changes, Cambridge University Press, United Kingdom, doi.org/10.1080/00107514.2015.1005682, 2014.

Rignot, E., Padman, L., MacAyeal, D., and Schmeltz, M.: Observation of ocean tides below the Filchner and Ronne Ice Shelves, Antarctica, using synthetic aperture radar interferometry: Comparison with tide model predictions, J. Geophys. Res.-Oceans, 105, 19615–19630, doi.org/10.1029/1999JC000011, 2000.

Rosier, S. H. R. and Gudmundsson, G. H.: Tidal bending of ice shelves as a mechanism for large-scale temporal variations in ice flow, The Cryosphere, 12, 1699–1713, doi.org/10.5194/tc-12-1699-2018, 2018.

Wild, C. T., Marsh, O. J., and Rack, W.: Differential interferometric synthetic aperture radar for tide modelling in Antarctic ice-shelf grounding zones, The Cryosphere, 13(12), 3171-3191, doi.org/10.5194/tc-13-3171-2019, 2019.

Table 1. Major tidal harmonic results for diurnal and semidiurnal constituents from harmonic analyses of sea level observations: year-long (2013) records from Cape Roberts (ROBT), and 17.04 day records (29 Jan. to 15 Feb. 2017) and 20.54 day records (29 Dec. 2018 to 18 Jan. 2019) from Jang Bogo Antarctic Research Station (JBARS) in the Ross Sea (see source details in Sect. 2). For the JBARS tidal harmonic analyses, the inference method was applied to separate out the K_1 (S_2) and P_1 (K_2) tidal constituents, using inference parameters estimated from the ROBT 2013 harmonic analysis.

Tidal constituents & characteristics		ROBT (2013) 369 days		JBARS (2017) 17.04 days		JBARS (2019) 20.54 days	
		Amp. (cm)	Pha. (°)	Amp. (cm)	Pha. (°)	Amp. (cm)	Pha. (°)
Diurnal	O_1	21.1	202	19.6	208	16.0	208
	K_1	20.5	217	16.3	214	14.9	216
	P_1	6.6	215	5.2	213	4.8	214
	Q_1	4.4	190	-	-	-	-
Semidiurnal	M_2	5.3	5	6.7	4	6.3	34
	S_2	4.9	309	6.4	329	5.7	320
	N_2	3.8	255	-	-	-	-
	K_2	1.8	315	2.4	333	2.4	328
F		4.1 (diurnal form)		2.7 (mixed, mainly diurnal)		2.6 (mixed, mainly diurnal)	
ADI (day)		0.57		0.23		0.30	
AT (day)		-2.30		-1.44		-2.87	

Note: Amp. denotes amplitude; Pha. denotes phase lag, referenced to 0° Greenwich; *F* is the amplitude ratio of the (K_1 + O_1)/(M_2 + S_2) tides; and *ADI* and *AT* denote the age of diurnal inequality and the age of the tide.

Table 2. Harmonic constants for 6 long-period tidal constituents, derived from harmonic analyses of year-long observations (2013) measured at the Cape Roberts sea level gauge (ROBT), using T_Tide (Pawlowicz et al., 2002)

Constituent		Amplitude (cm)	Amplitude standard error (cm)	Phase lag (º)	Phase lag standard error (º)	SNR
Solar annual	S_a	5.8	4.8	75	50	1.5
Solar semi-annual	S_{sa}	0.1	3.3	352	194	0.06
Lunar monthly	MS_m	0.4	3.5	57	254	0.02
	M_m	2.9	3.8	139	102	0.59
Lunar fortnightly	MS_f	1.2	3.0	281	189	0.14
	M_f	2.7	3.9	153	101	0.47

Phase lags are referenced to 0° Greenwich, and SNR denotes the signal-to-noise ratios.

Figure 1. Drifting ice, including icebergs and mobile sea ice, around the Jang Bogo Antarctic Research Station (JBARS), photographed on 29 Jan. 2017.

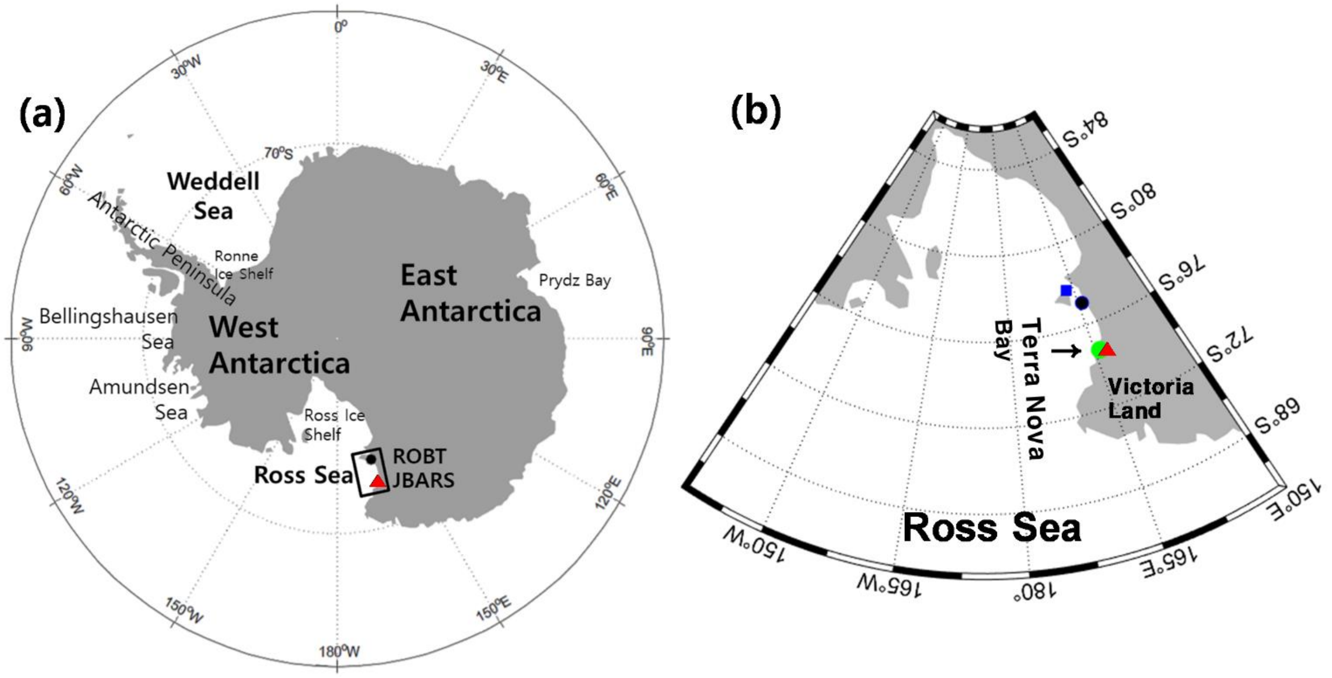

Figure 2. Maps showing (a) the locations of the two tidal observation stations employed in this study within a wider Antarctic context: Jang Bogo Antarctic Research Station (JBARS, ▲) and Cape Roberts (ROBT, ●); and (b) the case study station locations relative to two other (previous) temporary tidal observations stations, McMurdo Station (■), and Mario Zucchelli Station (●), in the Ross Sea.

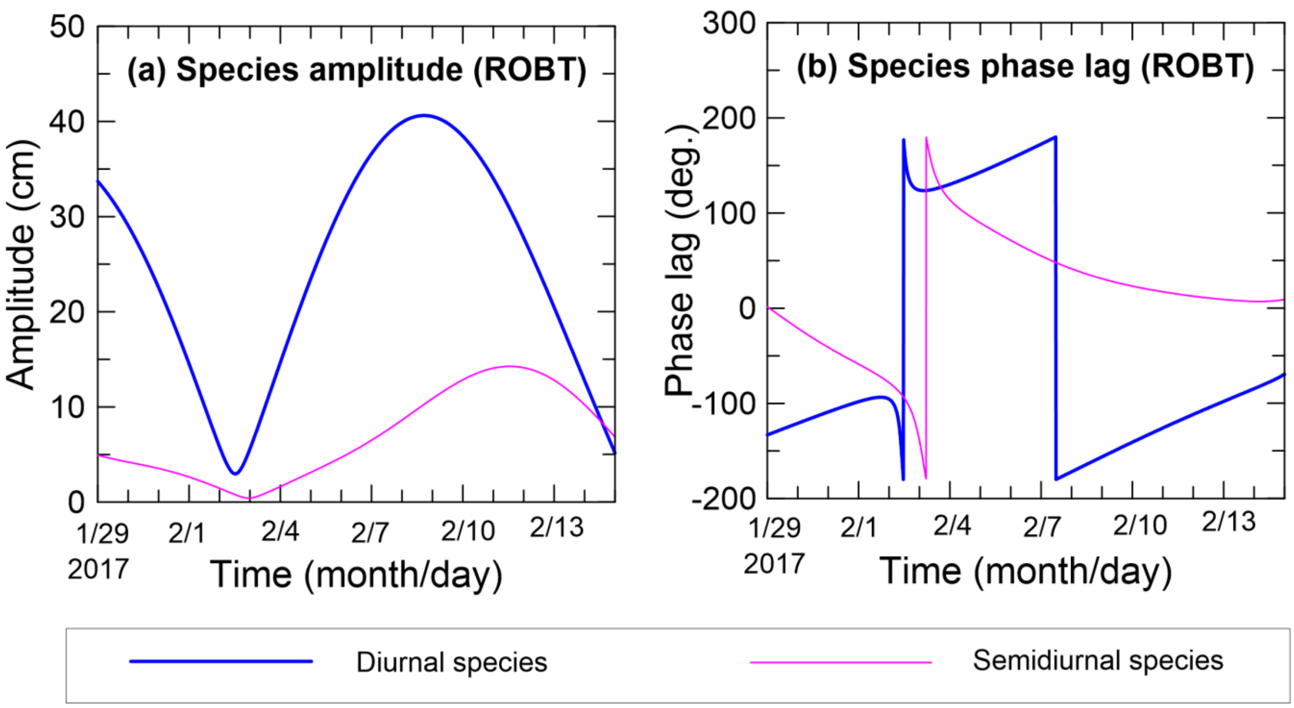

Figure 3. Modulated tidal (a) species amplitudes and (b) phase lags for the diurnal and semidiurnal tidal species, calculated from Cape Roberts (ROBT) tidal prediction data (29 Jan. to 14 Feb. 2017), using Appendix 1 Eqs. (A1) and (A3).

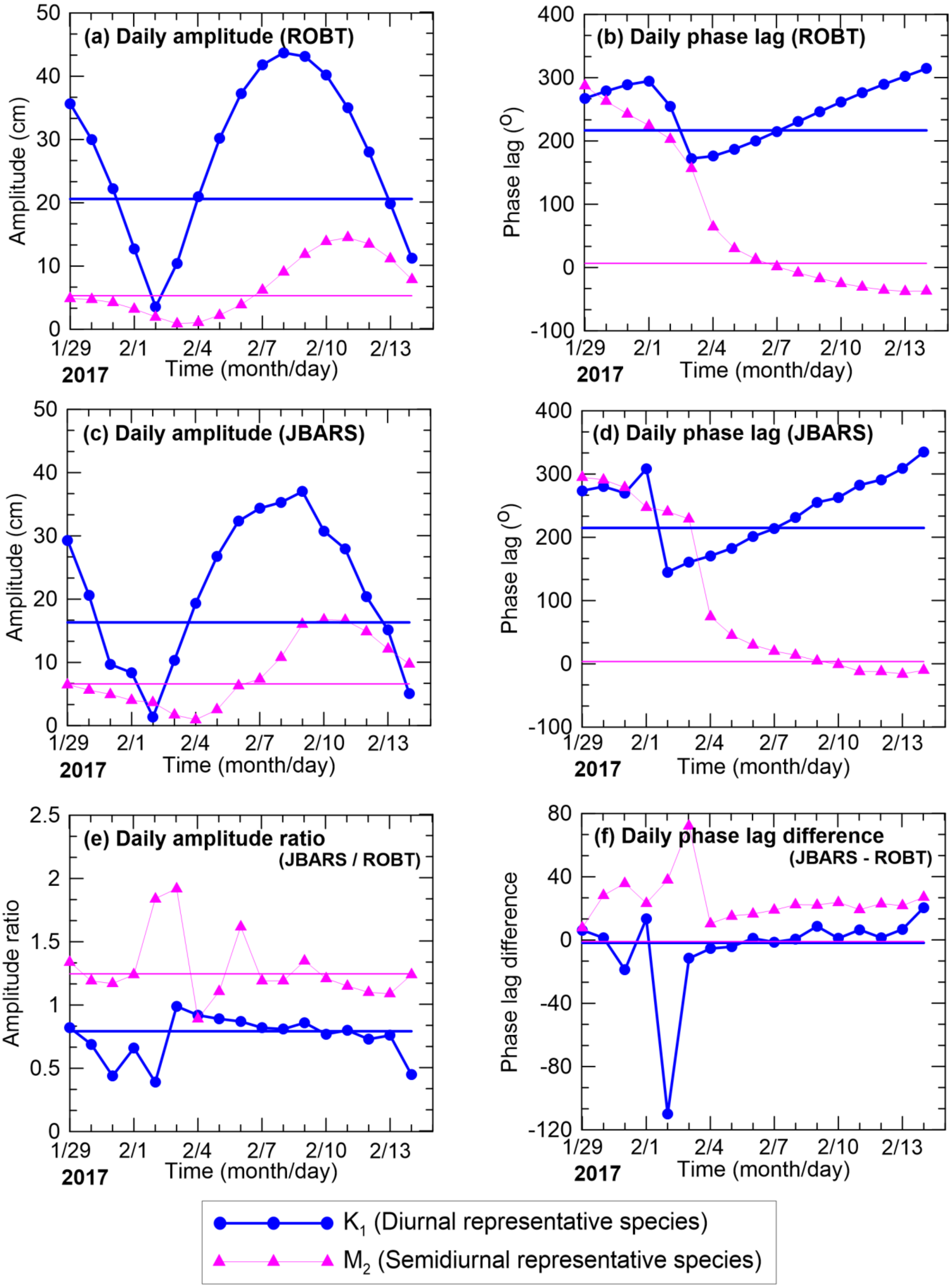

Figure 4. Daily amplitudes (a, c); phase lags (b, d); amplitude ratios (e); and phase lag differences (f) of the K_1 and M_2 tides (representative diurnal and semidiurnal tide species) at ROBT (a, b) and JBARS (c, d), and between JBARS and ROBT (e, f), calculated from 'daily' slices of the 29 Jan. to 14 Feb. 2017 ROBT tidal predictions and JBARS sea level observations. In addition, thick blue (K_1) and thin pink (M_2) horizontal lines in the panels indicate the amplitudes and phase lags derived from harmonic analyses of the 369 day 2013 ROBT sea level records (a, b) and of the 17 day 2017 JBARS sea level records (c, d), along with their amplitude ratios and phase lag differences (e, f).

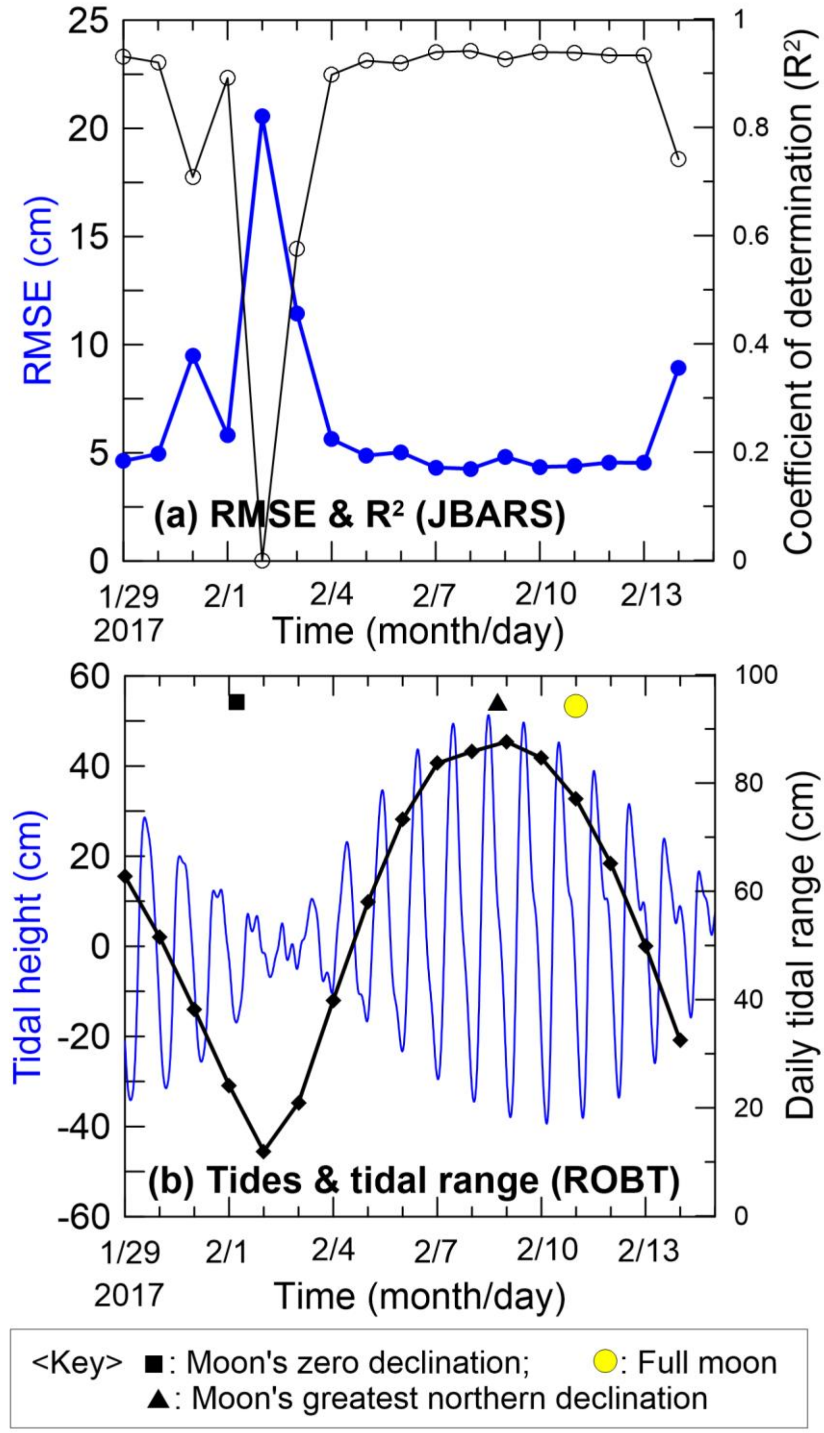

Figure 5. (a) Time series (29 Jan. to 14 Feb. 2017) of Root Mean Square Errors (RMSE, thick blue line with ●) and coefficients of determination (R^2, thin black line with ○) between JBARS 10 min interval sea level observations and the CTSM+TCC prediction datasets, generated for this site using harmonic analysis results from the JBARS daily (25 hr) sea level data slices and concurrent daily (25 hr) 2017 tidal prediction data slices and harmonic analysis results from ROBT station's year-long (2017) tidal predictions. (b) Time series of predicted 2017 tidal heights (thin blue line) and daily tidal ranges (thick black line with ♦) for ROBT, based on harmonic analysis of this station's 2013, 5 min interval sea level records, plus an indication of the moon's phase and declination.

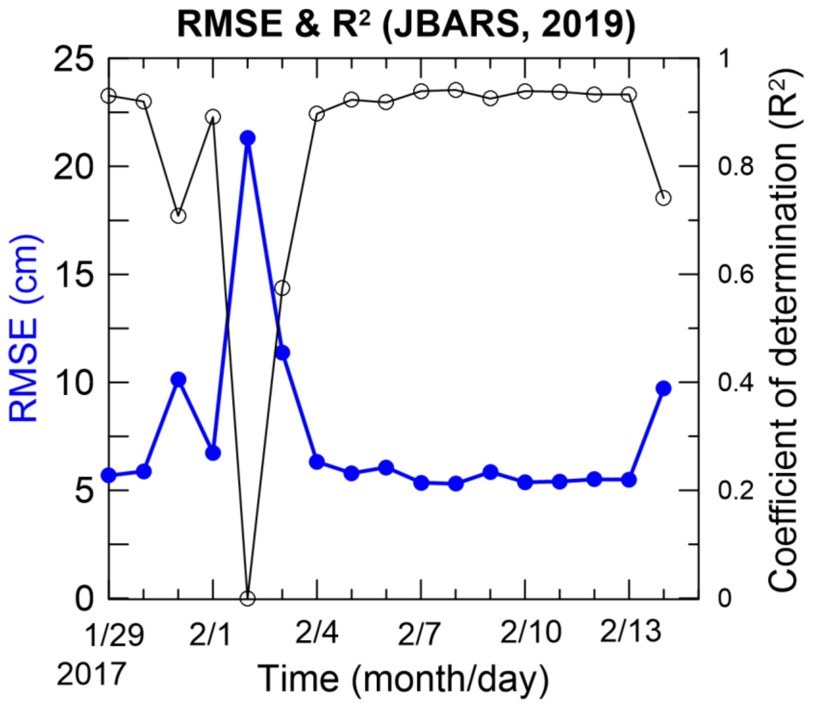

Figure 6. Time series of Root Mean Square Errors (RMSE, thick blue line with ●) and coefficients of determination (R^2, thin black line with ○) between JBARS 10 min interval sea level observations (29 Dec. 2018 to 18 Jan. 2019) and the CTSM+TCC prediction data sets generated for this site (using harmonic analysis results from daily (25 hr) summertime 2017 sea level data slices from JBARS along with concurrent daily (25 hr) tidal prediction slices and harmonic analysis results from ROBT station's year-long (2017) tidal predictions).

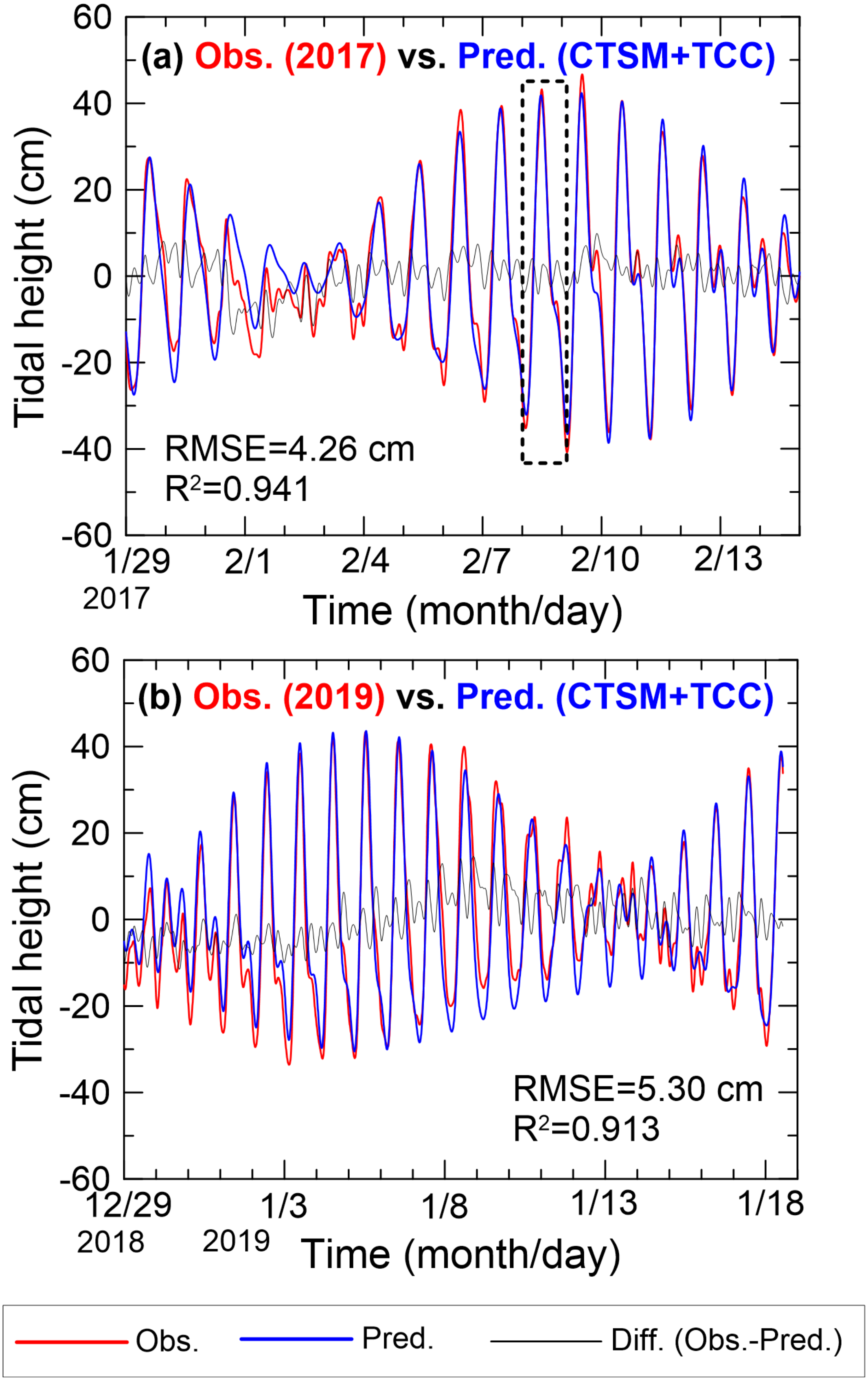

Figure 7. Time series of JBARS sea level observations (Obs.), predicted tidal heights (Pred.), and sea level residuals (Diff.) from (a) 29 Jan. to 14 Feb. 2017; and (b) 29 Dec. 2018 to 18 Jan. 2019. The JBARS predictions were generated via the CSTM+TCC method (using a daily (25 hr) slice of local sea level observations from 8 Feb. 2017 (dashed box in (a)), along with concurrent (to time periods a and b) ROBT predictions; and year-long (2017) 5 min interval ROBT tidal predictions). RMSE and R^2 denote the comparison Root Mean Square Errors and coefficients of determination, respectively.

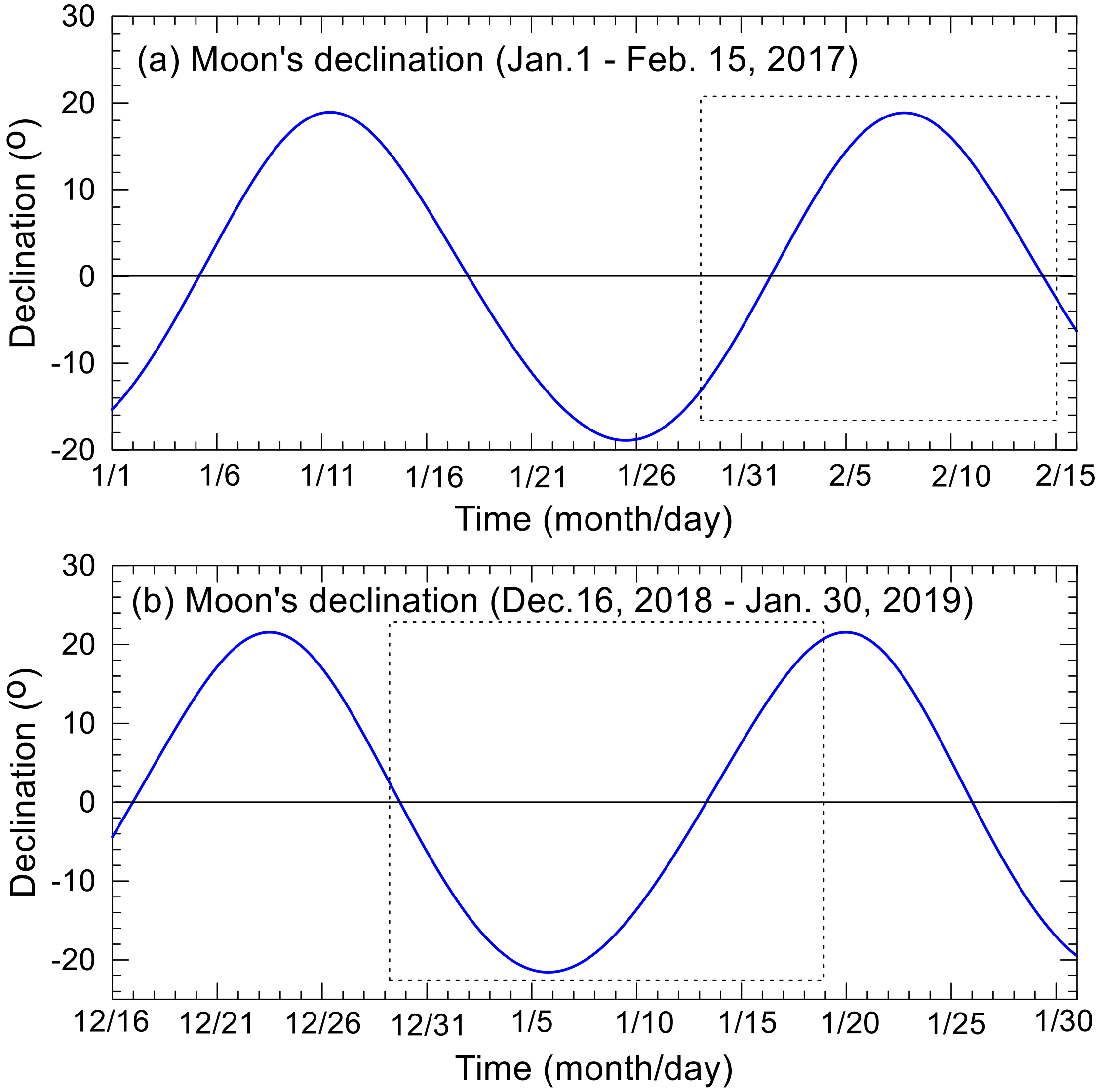

Figure 8. Time series of the Moon's declination, calculated at daily intervals for two observation periods: (a) 1 Jan. to 15 Feb. 2017; and (b) 16 Dec. 2018 to 30 Jan. 2019. Dashed boxes indicate the sea level observation windows examined in this study.

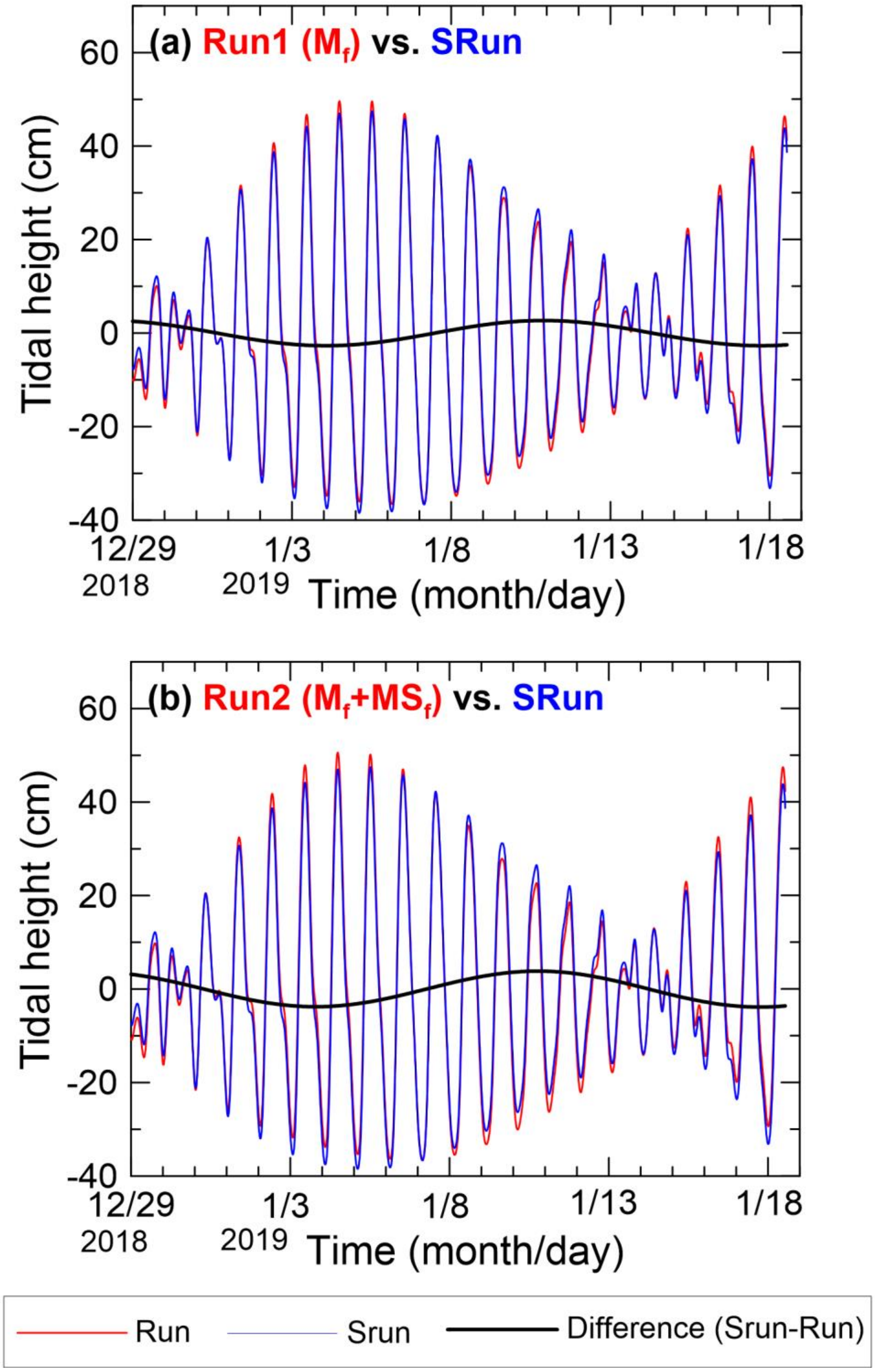

Figure 9. Time series of ROBT tidal predictions (a) made without long-period constituents (SRun, i.e. excluding the constituents listed in Table 2) versus with the M_f tide (Exp1); and (b) time series of ROBT tidal predictions made (SRun) without the long-period constituents versus (Exp2) with the MS_f and M_f tides. All predictions were generated based on tidal harmonic analysis results from the year-long (2013) ROBT sea level records.

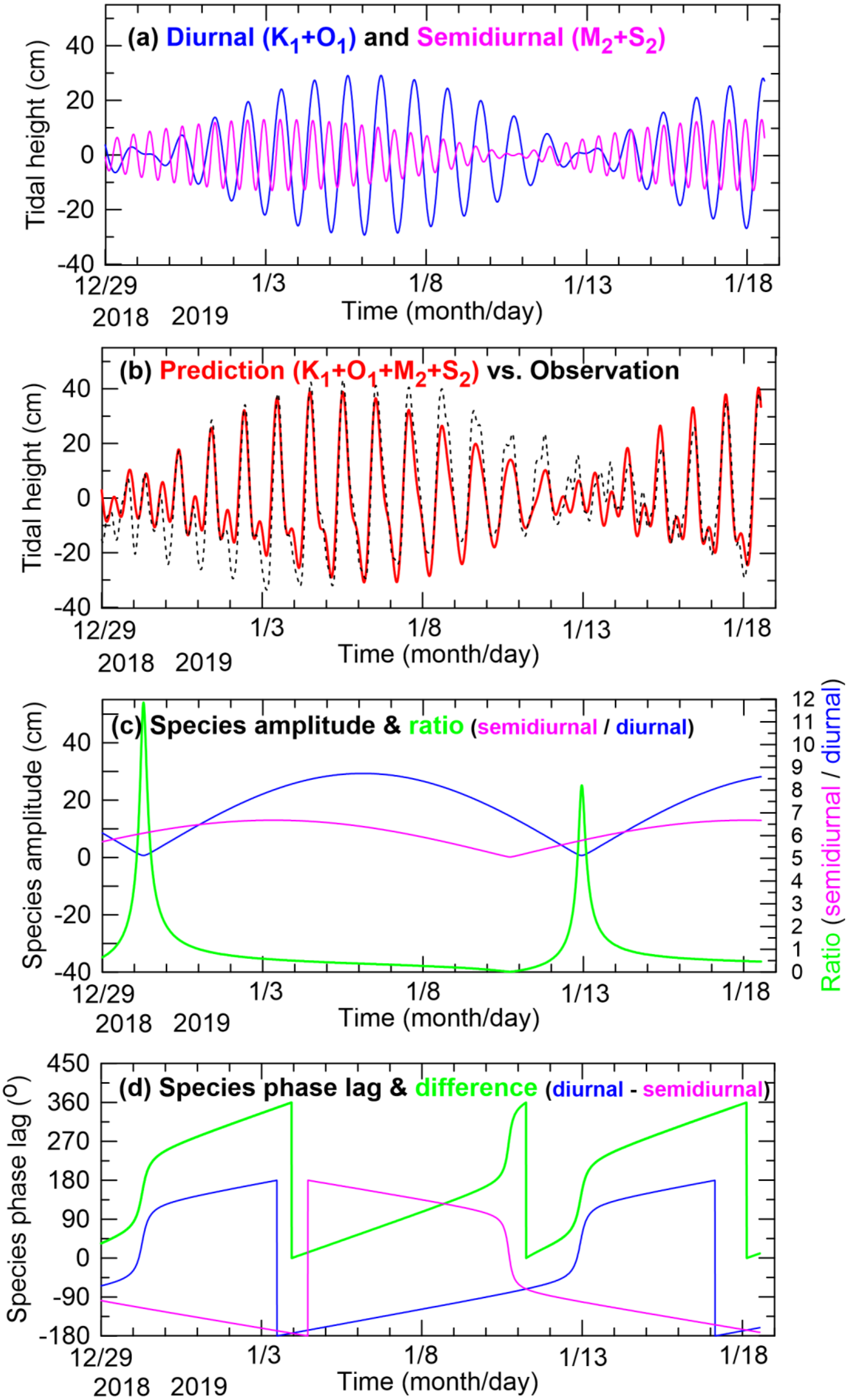

Figure 10. Time series (29 Dec. 2018 to 18 Jan. 2019) of (a) predictions of the diurnal (K_1+O_1) tides (blue line) and the semidiurnal (M_2+S_2) tides (magenta line) for JBARS; (b) their combined JBARS predictions (red line) and observations (black dashed line); (c) the ROBT diurnal (blue line) and semidiurnal (magenta line) species amplitudes and their ratio (green line); and (d) the ROBT diurnal (blue line) and semidiurnal (magenta line) species phase lags and their difference (diurnal – semidiurnal) (green line).

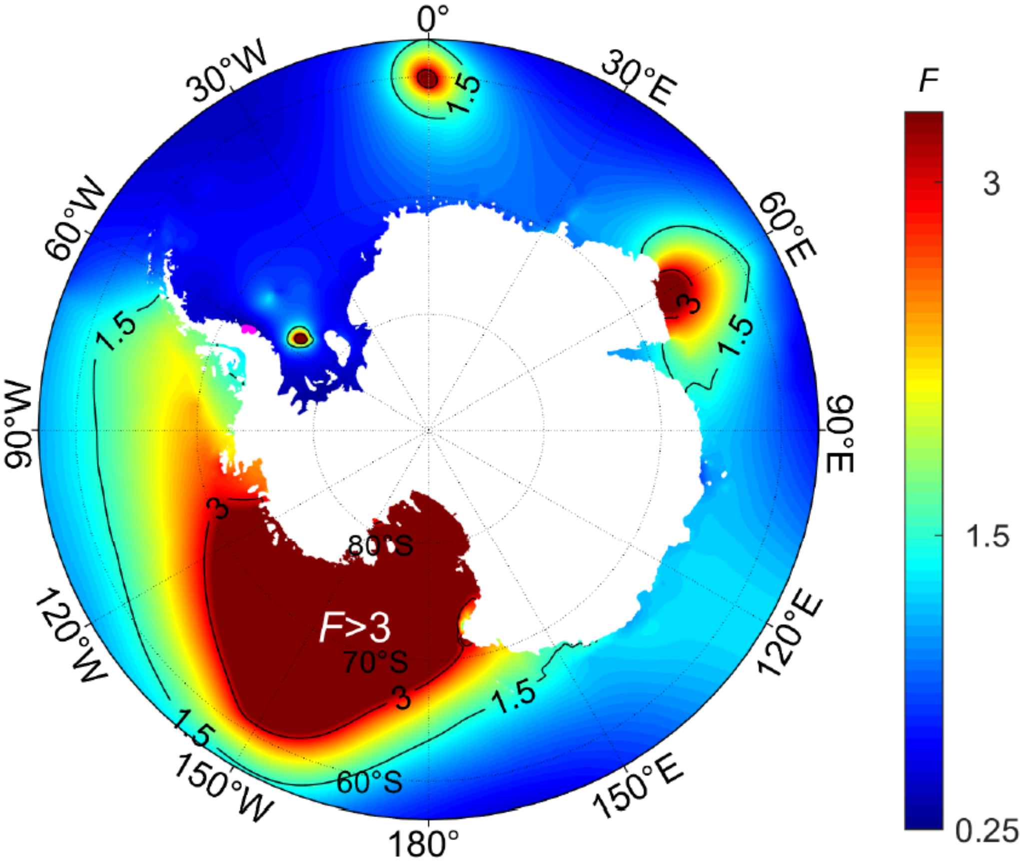

Figure 11. Distribution of tidal form factor (*F*) values around Antarctica. Note the magenta area (72°S) on the Antarctic Peninsula's Weddell Sea coast denotes the only area with a properly semidiurnal tide regime (*F*<0.25) in the Antarctic region.